Photonic Crystal Assisted 90° Waveguide Bend

H. Sami Sözüer, and H. Duygu Şengün
Izmir Institute of Technology, Department of Physics
Gulbahce Kampusu, Urla, Izmir, TURKEY
sozuer@photon.iyte.edu.tr

Received 11 August 2008

The 90° waveguide bend is an important component of optical circuit applications. We propose several models for such a bend, some of them assisted by a two-dimensional photonic crystal with a bandgap in the desired range of operating frequencies. We show that a photonic crystal assisted bend reduces bending loss by several orders of magnitude for transverse electric modes.

1. Introduction

Photonic crystal waveguide components are expected to play a significant role in photonic integrated circuit design because of the unique manner in which they confine electromagnetic radiation within various regions of space, dictated by deliberate design. Hence, it's possible to guide light along photonic crystal fibers[1], line defect waveguides (LDWG) [2,3], or design high quality optical microresonators[4]. Extensive research has been carried out designing and manufacturing LDWGs with remarkable customizable properties which makes them useful in a great variety of optical components, such as couplers[5] and add-drop filters[6] among others.

One serious shortcoming of LDWGs is their large sensitivity to imperfections introduced during manufacturing, which leads to high losses and limits their usefulness to guide light over long distances[7,8]. Furthermore, the high dispersion of 2D LDWGs also limits the bandwidth over which they can be used. To overcome these difficulties, Notomi *et. al.*[9] proposed using a 1D slab waveguide which is *not* periodic in the direction of propagation, and hence is much less lossy and has a much flatter dispersion. Light would indeed be guided with much less loss in such a waveguide due to lesser manufacturing imperfections as a result of its much simpler geometry, and the robustness of the 1D bandgaps to random manufacturing errors[10]. However, in an optical circuit, one would eventually want to bend the light, usually through a 90° angle due to the confined geometry. To bend light in such a waveguide in a trivial way would lead to unacceptably high bending losses. Bending light through sharp corners is another important forte of photonic crystals, and it is the purpose of this present work to propose an effective way of bending the light through 90° turns with little loss. To accomplish this one would want to switch to a 2D photonic crystal LDWG, bend the light through the required angle, and then switch back to the 1D slab waveguide again, possibly to travel for another long straight segment. For a 90° turn, the most convenient geometry is that of a square lattice.

There has been several optimized designs for employing a hexagonal lattice for 60° bends [11,12], and for 120° bends [3]. The guidance in these studies is photonic bandgap guidance as the index of refraction of the guiding region is lower than that of the cladding region. Ntakis *et. al.*[13] offer various bend designs to minimize loss around the bend, by deforming the geometry of the bend in various ways.

In this work we use a 2D structure to demonstrate the feasibility of such a design with TE modes. Since manufacturing silicon-silica binary photonic crystals is quite commonplace and mature[14,15], we report results of calculations for such structures, although clearly the approach is quite general and can be used for similar structures with lossless components with a sufficiently high dielectric contrast.

We tried several corner elements using a square photonic crystal LDWG to bend the light by removing one and two lines from the square lattice, with silicon rods in a silica background and the inverse structure with silica rods in a silicon background. When two rows of rods are removed from the 2D photonic crystal to form a LDWG, the propagation becomes multimodal inside the LDWG at the gap frequencies, leading to poor transmission because of increased scattering due to mode mismatch at the interface. Therefore we report here results for the LDWG corner element with only one row removed, which yields the lowest overall bending loss.

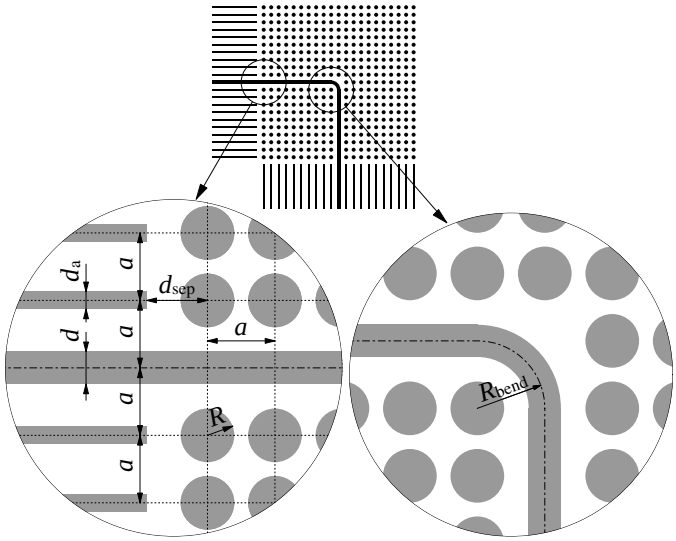

Fig. 1. The corner geometry (inset) and the geometrical details of the interface between the 1DWG and the LDWG.

2. Corner Element

In our proposed structure, shown in Fig. 1, light is bent in a 2D square lattice LDWG, formed by removing an L-shaped single row of rods from a square lattice of Si rods em-

bedded in a silica background. Since the 2D photonic crystal cornering element would be most effective *i.e.* yield the least bending loss if it has a large photonic bandgap at the range of operating frequencies, we look for the 2D lattice with the largest gap.

For the given index contrast, this structure has a respectable 20% photonic bandgap for TE modes ($E_z \neq 0$) centered at $\tilde{\omega} \equiv= \omega a/2\pi c = 0.2667$ when $\tilde{R} \equiv 2\pi R/a = 1.5$ as shown in Fig. 2. Our proposed system to guide light, then, has 3 essential elements:

I Single mode guiding at a particular frequency window over relatively long distances.
II Coupling into a 2D photonic crystal LDWG with a single guided mode
III Bending light through 90° in a confined geometry, which requires that the 2D photonic crystal have a large bandgap at the operating frequency.

2.1. *2D Square Lattice*

The single most important element in this scheme is that the 2D photonic crystal have a wide bandgap at the operating frequency, we start with selecting the 2D photonic crystal first, and then choose the LDWG and the 1DWG elements that minimize the bending loss. To model the 2D square lattice, we use the planewave expansion method which is quite satisfactory for 2D problems. For TE modes ($E_x = E_y = 0,\ E_z \neq 0$), the solutions are of the form

$$E_z(x, y, t) = E_{0z}(x, y)e^{i(\mathbf{k}\cdot\mathbf{r}-\omega t)} \tag{1}$$

This yields the generalized eigenvalue equation

$$|\mathbf{k} + \mathbf{G}|^2 E_z(\mathbf{G}) = \frac{\omega^2}{c^2} \sum_{\mathbf{G}'} \epsilon(\mathbf{G} - \mathbf{G}')E_z(\mathbf{G}') \tag{2}$$

where

$$\mathbf{G} = \frac{2\pi}{a} n_x \hat{\mathbf{x}} + \frac{2\pi}{a} n_y \hat{\mathbf{y}} \quad n_x, n_y = 0, \pm 1, \pm 2, \ldots$$

is a reciprocal lattice vector and $\mathbf{k}$ is a vector in the first Brillouin zone. This can be converted into an ordinary eigenvalue problem of the form $\mathsf{A}\mathsf{x} = (\omega^2/c^2)\mathsf{x}$ with

$$\begin{aligned} \mathsf{A}_{\mathbf{G}\mathbf{G}'} &= |\mathbf{k} + \mathbf{G}|\, [\epsilon^{-1}]_{\mathbf{G}\mathbf{G}'}\, |\mathbf{k} + \mathbf{G}'| \\ \mathsf{x}_{\mathbf{G}} &= |\mathbf{k} + \mathbf{G}|\, E_z(\mathbf{G}) \end{aligned} \tag{3}$$

where ϵ^{-1} is the inverse of the matrix $\epsilon_{\mathbf{G}\mathbf{G}'} = \epsilon(\mathbf{G} - \mathbf{G}')$. For circular rods,

$$\epsilon(\mathbf{G}) = \epsilon_b \delta_{\mathbf{G}\mathbf{0}} + (\epsilon_a - \epsilon_b)\frac{\pi R^2}{a^2} \frac{2J_1(GR)}{GR} \tag{4}$$

where $J_1(x)$ is the Bessel function of order 1, and for square rods of side $2R$,

$$\epsilon(\mathbf{G}) = \epsilon_b \delta_{\mathbf{G}\mathbf{0}} + (\epsilon_a - \epsilon_b)\frac{4R^2}{a^2} \frac{\sin(G_x R)}{G_x R} \frac{\sin(G_y R)}{G_y R} \tag{5}$$

The largest bandgap we find is around 20%, with circular Si rods in a silica background at a Si filling ratio of $f = 0.17$ and radius $\tilde{R} = 1.5$. The band structure with these parameters

is displayed in Fig. 3c. With square Si rods in a silica background, there is a respectable 19% bandgap. The bandgap for circular silica rods in Si is much smaller, and there were no gaps with silica square rods in Si. Now that we know what the optimum 2D photonic

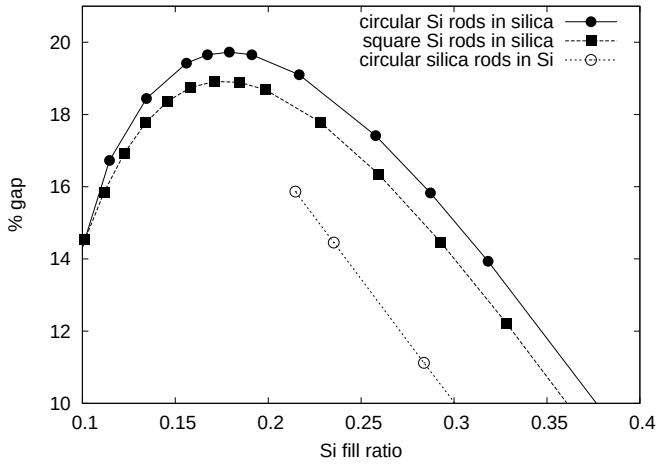

Fig. 2. The relative gap width vs the normalized radius $\tilde{R}$ for a 2D photonic crystal made of silicon rods of dielectric constant of $\epsilon_a = 13$ in a silica background with $\epsilon_b = 2.25$. The maximum bandgap occurs at $\tilde{R} = 1.5$.

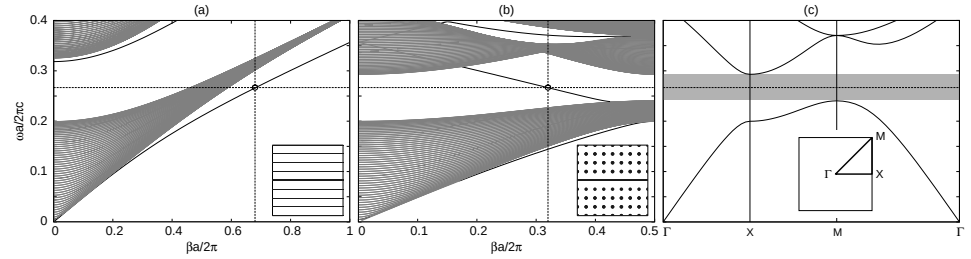

Fig. 3. Band structures for the three components of the bend. (a) The propagation modes for the 1DWG made of silicon slabs of thickness $\tilde{d}_{\rm Si} = 1.125$, and with dielectric constant of $\epsilon_a = 13$ immersed in a silica background with $\epsilon_b = 2.25$. The defect is formed by removing one row of dielectric slabs and by placing a dielectric slab of thickness $\tilde{d} \equiv 2\pi d/a = 2$. The finely spaced gray bands are those of unguided radiation modes. The centergap frequency $\omega a/2\pi = 0.2667$ and the corresponding propagation constant $\beta a/2\pi = 0.78$ are indicated by the cross-hair. The gray bands correspond to non-localized radiation modes. The solid curves are those of localized propagation modes. (b) The localized propagation modes of a line defect waveguide with a core for a 2D photonic crystal made of silicon rods of radius $\tilde{R} = 1.5$, immersed in a silica background. The line defect is formed by removing one row of dielectric rods and by extending the core of the 1DWG. (c) The band structure for the perfect 2D photonic crystal with the path traversed in the Brillouin Zone shown in the inset. All bands are for TE modes.

crystal is for the given dielectric materials, we can now decide what kind of a waveguide can be formed out of this photonic crystal that will best match the 1DWG.

2.2. *The LDWG*

The LDWG is formed by removing one row of Si rods and replacing with a Si slab of normalized thickness $\tilde{d} = 2$ is shown in Fig. 1. The LDWG is modeled using the supercell method with a supercell size of $A_x \times A_y$, where $A_x = a$ and $A_y = 61a$ to ensure that the guided mode is well contained within the supercell. For TE modes ($E_x = E_y = 0,\ E_z \neq 0$), propagating along the x-axis with propagation vector $\boldsymbol{\beta} = \beta\hat{\mathbf{x}}$, the solutions are of the form

$$E_z(x, y, t) = E_{0z}(x, y)e^{i(\beta x - \omega t)} \tag{6}$$

This yields the generalized eigenvalue equation

$$|\boldsymbol{\beta} + \mathbf{G}|^2 E_z(\mathbf{G}) = \frac{\omega^2}{c^2} \sum_{\mathbf{G}'} \epsilon(\mathbf{G} - \mathbf{G}')E_z(\mathbf{G}') \tag{7}$$

where

$$\mathbf{G} = \frac{2\pi}{a} n_x \hat{\mathbf{x}} + \frac{2\pi}{(2M+1)a} n_y \hat{\mathbf{y}} \quad n_x, n_y = 0, \pm 1, \pm 2, \ldots$$

.

This can be converted into an ordinary eigenvalue problem of the form $\mathsf{A}\mathsf{x} = (\omega^2/c^2)\mathsf{x}$ with

$$\begin{aligned} \mathsf{A}_{\mathbf{GG}'} &= |\boldsymbol{\beta} + \mathbf{G}|\, [\epsilon^{-1}]_{\mathbf{GG}'}\, |\boldsymbol{\beta} + \mathbf{G}'| \\ \mathsf{x}_{\mathbf{G}} &= |\boldsymbol{\beta} + \mathbf{G}|\, E_z(\mathbf{G}) \end{aligned} \tag{8}$$

where ϵ^{-1} is the inverse of the matrix $\epsilon_{\mathbf{GG}'} = \epsilon(\mathbf{G} - \mathbf{G}')$, with

$$\begin{aligned} \epsilon(\mathbf{G}) = \epsilon_b \delta_{\mathbf{G0}} &+ (\epsilon_a - \epsilon_b)\frac{d}{(2M+1)a} \frac{\sin(G_y d/2)}{(G_y d/2)} \\ &+ (\epsilon_a - \epsilon_b)\frac{\pi R^2}{(2M+1)a^2} \frac{2J_1(GR)}{GR} \left[\sum_{j=1}^{M} 2\cos(G_y a j) \right] \end{aligned} \tag{9}$$

where the second term is due to the core region at the center of the waveguide, and the term in square brackets is the structure factor for the cylinders.

The dispersion relation is displayed in Fig. 3b. Since the imaginary part of the wave vector is maximum near the center of the bandgap, the operating frequency is expected to be around the centergap value of $\tilde{\omega} = 0.2667$. However, since the incident wave is along the X-direction, and confining light in this direction would require a large imaginary part for the wave vector, an operating frequency near the center of the gap at the X-point yields a bending loss that is appreciably less than that at the centergap frequency.

2.3. *1DWG*

The band structure of the 1DWG portion is again modeled by assuming a wave of the form

$$E_z(x, y, t) = E_{0z}(y)e^{i(\beta x - \omega t)} \tag{10}$$

for TE modes ($E_x = E_y = 0,\ E_z \neq 0$) propagating in the x-direction with propagation vector $\boldsymbol{\beta} = \beta\hat{\mathbf{x}}$. Inserting this into Maxwell's equations, and using a supercell of size $2M+1$ along the y-axis, one obtains the generalized eigenvalue equation

$$(\beta^2 + G^2)E_z(G) = \frac{\omega^2}{c^2}\sum_{G'}\epsilon(G-G')E_z(G') \tag{11}$$

where

$$G = \frac{2\pi}{(2M+1)a}i \quad i = 0, \pm 1, \pm 2, \ldots$$

. This can be converted into an ordinary eigenvalue problem of the form $\mathsf{A}\mathsf{x} = (\omega^2/c^2)\mathsf{x}$ with

$$\begin{aligned} \mathsf{A}_{GG'} &= \sqrt{\beta^2+G^2}\ [\epsilon^{-1}]_{GG'}\ \sqrt{\beta^2+G'^2} \\ \mathsf{x}_G &= \sqrt{\beta^2+G^2}\,E_z(G) \end{aligned} \tag{12}$$

where ϵ^{-1} is the inverse of the matrix $\epsilon_{GG'} = \epsilon(G-G')$, with

$$\begin{aligned} \epsilon(G) = \epsilon_b\delta_{G0} &+ (\epsilon_a-\epsilon_b)\frac{d}{(2M+1)a}\frac{\sin(Gd/2)}{(Gd/2)} \\ &+ (\epsilon_a-\epsilon_b)\frac{d_a}{(2M+1)a}\frac{\sin(Gd_a/2)}{(Gd_a/2)}\left[\sum_{j=1}^{M}2\cos(Gaj)\right] \end{aligned} \tag{13}$$

where the second term is due to the core region at the center of the waveguide, and the term in square brackets is the structure factor for the supercell.

The dispersion relation ω vs β is displayed in Fig. 3a. The method and some of the pitfalls have been discussed elsewhere[16]. We obtain satisfactory convergence for about 100 plane waves per unit cell for the LDWG and for 25 plane waves per unit cell for the 1DWG.

3. Mode Matching

The band structures in Fig. 3 show that single mode operation in both the 1DWG and the LDWG is possible for frequencies in the bandgap of the 2D photonic crystal. However, since light passes from the 1DWG to the corner element and then, after turning, reenters the 1DWG region, one wants minimum reflection/diffraction at the entry and exit interfaces. To that end, two conditions are critically important:

I. The mode profiles of the 1DWG and the LDWG must be matched.

II. The dispersion relation $\omega(\beta)$ in the 1DWG and the LDWG must be matched.

These require careful tuning of the geometrical parameters d and R Furthermore, the spacing between the 1DWG and the 2D corner element must to be carefully adjusted to ensure minimum reflection at the entry and exit interfaces.

To quantify the degree to which the mode profiles of the 1DWG and the LDWG match, we define the relative mode profile mismatch between the two media as

$$\delta(x) \equiv \sqrt{\frac{\int_{-A_y/2}^{A_y/2}dy[E_{1z}(y)-E_{2z}(x,y)]^2}{\int_{-A_y/2}^{A_y/2}dy[E_{1z}(y)]^2}}$$

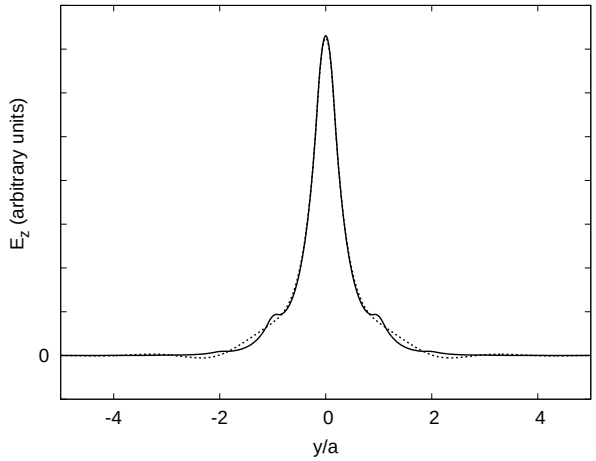

Fig. 4. The localized propagation mode $E_z(y)$ (dashed curve), of a 1D photonic crystal waveguide made of silicon slabs of thickness $\tilde{d}_{\rm Si} = 1.125$, and with dielectric constant of $\epsilon_a = 13$ immersed in a silica background with $\epsilon_b = 2.25$, compared with $E_z(-a/2, y)$ (solid curve), the cross section at $x = -a/2$, of the mode of the 2D LDWG at the centergap frequency $\tilde{\omega} = 0.2667$.

where $E_{1z}(y)$ is the mode profile of the 1DWG and $E_{2z}(x_0, y)$ is the mode profile of the LDWG at fixed x_0. We search for a value of x that minimizes $\delta(x)$. Because of the peri-

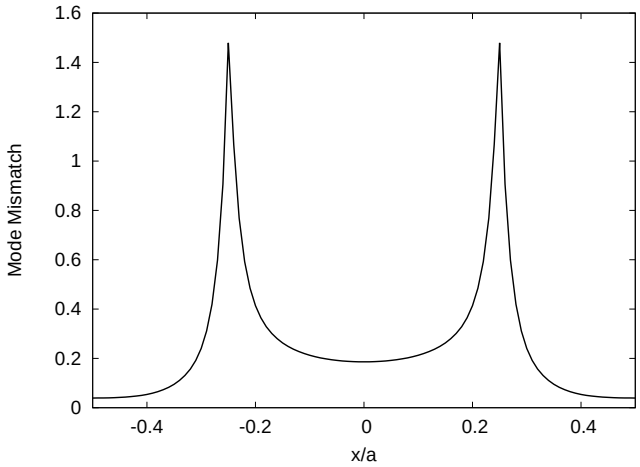

Fig. 5. The relative mode mismatch $\delta(x)$ between the modes of the 1D waveguide and that of 2D LDWG as a function of x. The mismatch is smallest at $x = -a/2$. Maximum coupling is obtained when the spacing between the 1D waveguide and the center of the rods in the 2D structure is $\approx 0.9a$

odicity in the x-direction, x can assume values in the interval $(-a/2, a/2)$. A plot of $\delta(x)$ is shown in Fig. 4. The value of $\delta(x)$ is minimum at the point $x = -a/2$, and a plot of the two modes is shown in Fig.5. So it seems that setting the separation between the end of the 1DWG and the center of the first column of rods in the 2DWG, $d_{\rm sep}$ to $a/2$ would yield the

best match, but we can do even better. We made FDTD calculations for various separations and found that the maximum transmission is obtained by setting $d_{\text{sep}} = 0.9a$.

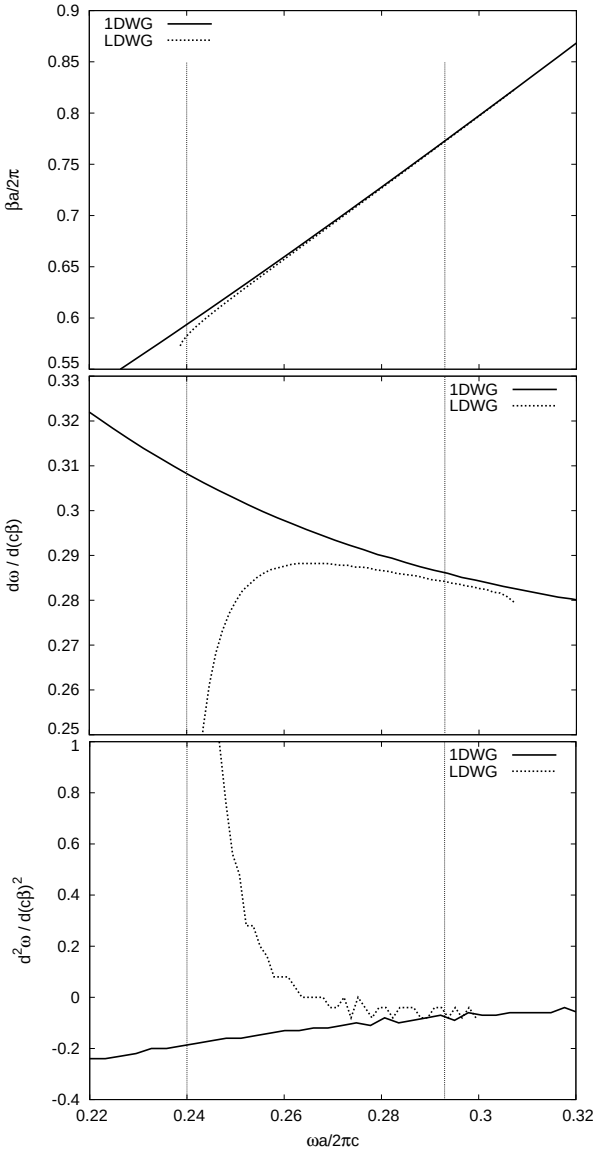

Fig. 6. The propagation constant β vs the frequency ω, the group velocity $v_g = d\omega/d\beta$ vs ω, and $d^2\omega/d\beta^2$ vs ω plots for the 1DWG and LDWG. The dotted vertical lines mark the edges of the 2D photonic band gap. The β values for the LDWG are the unfolded values from Fig. 3b.

Besides matching the mode profiles, one would also want to match the dispersion relation $\omega(\beta)$ in the two media. Looking at Fig. 6, we see that for frequencies within the

bandgap, the values of β differ by only a small amount at the same frequency, while the values of the group velocity $v_g = d\beta/d\omega$ differ by about 2% for the two media at the centergap frequency. The second derivative, $d^2\omega/d\beta^2$ is related to waveguide dispersion, and again, the values for the two media are reasonably close, although a percentage comparison is not too meaningful since the values are close to zero at the centergap frequency.

3.1. *FDTD Simulation Results*

The band structures calculated so far can be used to gain insight into the problem and decide which structures hold promise, but the final step has to be the actual time domain simulation to prove, without a doubt, that the corner design actually works.

Above, we can figure out parameters for our proposed structure and also we know now which frequencies are guided and which are not. We would like to know exactly how much power makes it around the bend, the rest being either reflected or radiated away. For that we need to compute the fluxes through a line segment with the width of the waveguide. We do this once for the straight 1D PhC WG, and once again after the bend. The FDTD simulations have been performed using MEEP[17], which allows great flexibility in using custom sources.

To obtain accurate transmission results, we made sure the straight sections of the bend are identical to the reference 1D PhC WG. Since we are primarily interested in TE modes for which $E_z \neq 0$, as the source, we use a current source of the form

$$\mathbf{J}(\mathbf{r}, t) = \delta(x - x_s)\, E_{1z}(y, \omega)\, \exp\left[\frac{-(t - t_0)^2}{2\sigma^2}\right] \exp(-i\omega t)\, \hat{\mathbf{z}} \tag{14}$$

which is a monochromatic source of frequency ω, located at $x = x_s$ and enveloped in a Gaussian packet with width $\Delta\omega = 1/\sigma$ in the frequency domain. $E_{1z}(y, w)$ is the guided mode of the 1D PhC WG at the center frequency ω Its Fourier coefficients are obtained by solving the eigenproblem Eq. 11, and its inverse FT is calculated as either a sine or a cosine series depending on whether the source is even or odd. The current source must be in the z-direction in order to excite TE modes.

It's tempting to instead use a point source for even modes and two antisymmetric point sources for odd modes, for the sake of simplicity. However, depending on the frequency, one would then have to use an unusually long straight segment for the 1D PhC WG before the bend, in order to have all of the unguided modes radiate out of the 1D PhC WG. Our mode source excites only one mode, just itself, so the initial straight segment can be made very short, thereby significantly reducing the simulation time, in addition to yielding much more accurate results for transmission.

The transmission of the bend then can be defined as the ratio of the total output flux P_o measured after the bend, to the total input flux P_i for the corresponding straight WG, which is given by $T = -10 \log_{10}(P_o/P_i)$.

Since the source is Gaussian, in principle it would never "end" and the simulation would take forever. For the flux calculations, we ran our simulations until well after the fields have decayed to 1/10,000th of their peak values at the end of the waveguide where the flux-regions have been placed.

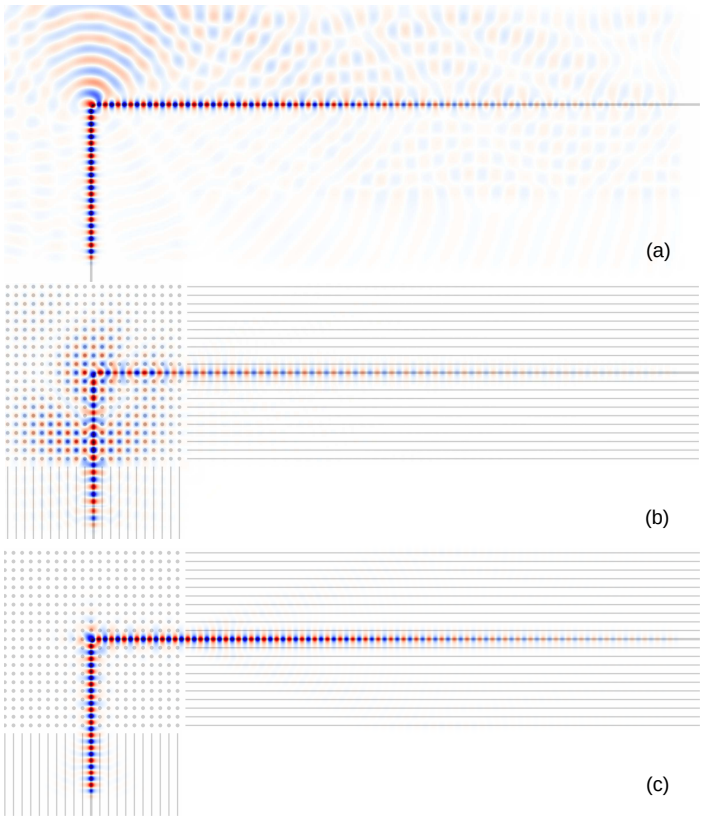

Fig. 7. FDTD simulations of (a) single silica slab waveguide bend, and the photonic crystal assisted bend (b) at the the frequency of $\tilde{\omega} = 0.23889$ which is below the bandgap, and (c) at the centergap frequency of $\tilde{\omega} = 0.2667$. The bending radius of the core centerline is twice the width of the core for each case. The wave is a gaussian with width $\Delta\tilde{\omega} = 0.1$. In each case, the 1D waveguide is excited with a current source that matches the guided mode at that frequency.

In Figure 7a, we present a snapshot from our simulations of a single Si core in silica, without photonic crystal assistance. As would be expected, there is large leakage at the corner. Figure 7b is a snapshot with photonic crystal assistance, but when the frequency $\tilde{\omega} = \omega a/2\pi c = 0.23889$ is *outside* the band gap $0.240426 < \tilde{\omega} < 0.293049$ of the 2D square lattice. The radiation penetrates visibly into the 2D structure and there is serious leakage. By contrast, Figure 7c is a snapshot from the simulation at the centergap frequency $\tilde{\omega} = 0.2667$. This time, there is no visible penetration into the 2D corner element, and the transmission is nearly lossless.

Figure 8 shows the transmission through the photonic crystal assisted 90° bend as a function of frequency, for $R_{\text{bend}} = d$ (blank squares), and for $R_{\text{bend}} = 2d$ (blank circles), where d is the width of the core region. Also shown are the transmission curves for a slab WG without photonic crystal assistance for $R_{\text{bend}} = d$ (filled squares) and for $R_{\text{bend}} = 2d$ (filled circles). The transmission of the photonic crystal assisted bend is largest for frequencies inside the 2D photonic crystal bandgap which lies in the range $0.240426 <$

$\tilde{\omega} < 0.293049$.

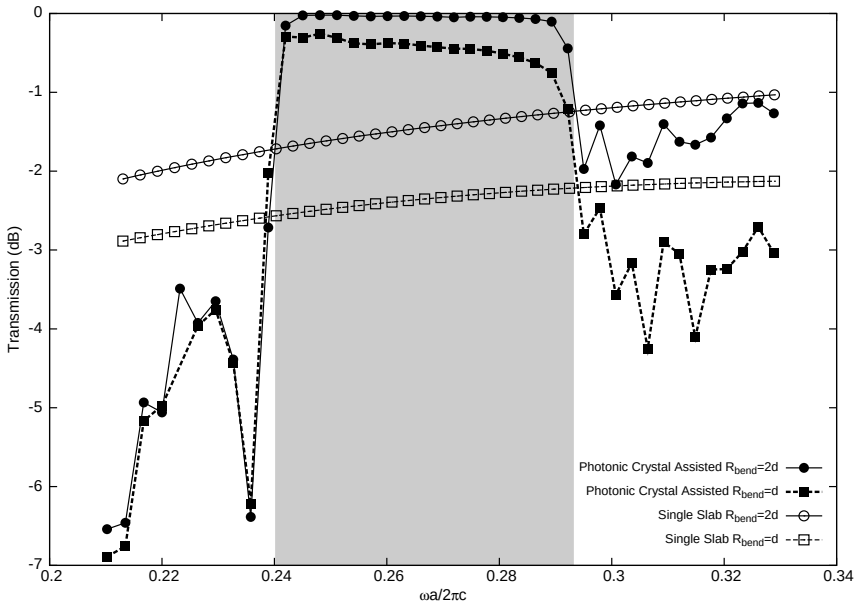

Fig. 8. Transmission through the photonic crystal assisted 90° bend as a function of frequency for $R_{\text{bend}} = d$ (filled squares), and for $R_{\text{bend}} = 2d$ (filled circles), where d is the width of the core region. Also shown are the transmission curves for a slab waveguide without photonic crystal assistance for $R_{\text{bend}} = d$ (blank squares), and for $R_{\text{bend}} = 2d$ (blank circles). The transmission of the photonic crystal assisted bend is largest for frequencies inside the 2D photonic crystal bandgap which lies in the range $0.240426 < \tilde{\omega} < 0.293049$, shown as a lightly shaded band. Further, within the gap region, transmission is greatest near $\tilde{\omega} \approx 0.25$, close to the center frequency of the X-gap. At this frequency, the bending loss for $R_{\text{bend}} = 2d$ is 0.0004 which corresponds to a 1000-fold reduction compared to that of single slab waveguide with the same bending radius. The minimum in bending loss occurs at a frequency close to the center of the X-gap rathe than the center of the total gap because the incident wave is in the X-direction inside the 2D LDWG and the imaginary part of its wave vector in the X-direction is largest at the centergap frequency of the X-point.

4. Alternate Structures

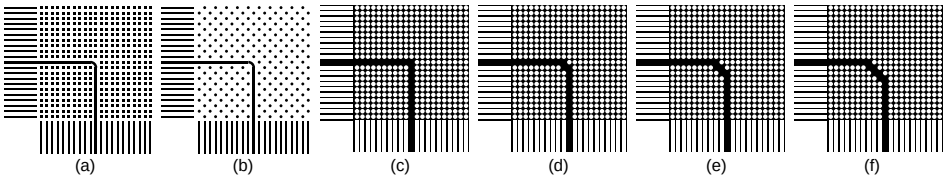

Fig. 9. Some of the alternate corner structures also considered as corner elements. (a) Silicon square rods arranged in square lattice, in silica. (b) Silicon circular rods arranged in checkerboard lattice, in silica. (c) (d) (e) and (f) Silica circular rods arranged in square lattice in silicon, with various bending geometries.

We tried several other corner geometries some of which are displayed in Fig. 9. The most successful was the silicon square rod in silica in Fig. 9a, with the periodicity of the square lattice. The transmission as a function of ω was practically identical to that of circular rods, displayed in Fig. 8. This result leads us to believe that the corner geometry would be quite robust to manufacturing errors as the transmission is quite insensitive to a change in shape of the rods.

Another interesting corner element can be constructed by turning the square lattice by 45°, yielding the "checkerboard lattice." The transmission for this corner element, displayed in Fig. 10, wasn't as high as the similar structure in the square lattice. This can be attributed largely to the more complicated interface between the 1DWG and the LDWG of the corner element, which makes it difficult to match the mode profile, resulting in increased scattering at the entry and exit interfaces of the corner element.

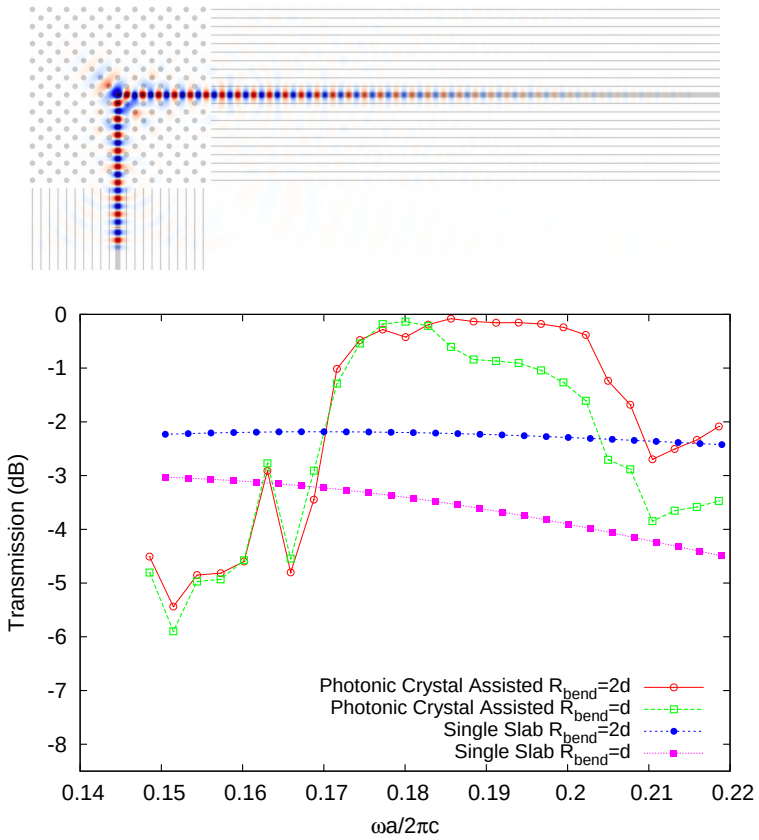

Fig. 10. Real time simulation (top) and the transmission through the "checkerboard" photonic crystal assisted 90° bend as a function of frequency $R_{\text{bend}} = d$ (blank squares), and for $R_{\text{bend}} = 2d$ (blank circles), where d is the width of the core region. Also shown are the transmission curves for a slab WG without photonic crystal assistance for $R_{\text{bend}} = d$ (filled squares) and for $R_{\text{bend}} = 2d$ (filled circles). The transmission of the photonic crystal assisted bend is largest for frequencies inside the 2D photonic crystal bandgap which lies in the range $0.170006 < \tilde{\omega} < 0.207217$.

The structures in Fig. 9c-9f, with silica rods in a silicon background, did not yield high transmission. This was mainly due to the fact that the propagation in the 2D segment is single mode only over a narrow range of frequencies opened up by a band anticrossing, shown in Fig. 11. In addition, the propagation inside the 1DWG is also multimode at the bandgap frequencies. The result is high scattering losses at the interfaces, leading to poor transmission, making these structures unsuitable for consideration as a corner element.

One might be tempted to think that increasing the length of the diagonal element, as in Fig 9f might increase transmission, by making the bend more "smooth," but quite to the contrary, the transmission is actually *reduced*, because the diagonal portion can be considered to be a different waveguide with its own dispersion relation and its own mode profile. Thus it introduces yet another pair of interfaces between the modes in the X-direction and those in the M-direction for the light to scatter from.

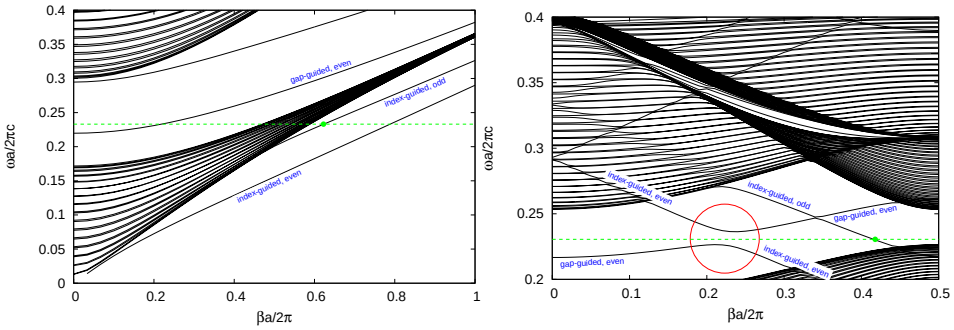

Fig. 11. Band structure for the 1DWG (left), and the 2D LDWG (right), formed by removing a row of silica rods in a square lattice. $R_{rod} = 3$. The band anticrossing for the LDWG is indicated by the red circle. The green line and the green dot mark the operating frequency $\omega = 0.232$ and the wave vector with an unfolded value of $\beta = 0.54$.

5. Conclusion

For TE modes in a 2D setting, we have shown that a low-loss hybrid 1D-2D waveguiding system, employing a square lattice for the corner element and a 1D PhC waveguide for the straight sections, is realizable for consideration in photonic integrated circuits. The bending loss can be as little as $\sim 10^{-4}$. Among the various geometries considered, we found that the structure consisting of circular silicon rods embedded in a silica background yields the highest transmission. It remains to be seen whether a 3D version of this approach, with a slice of appropriate thickness on top of a substrate will similarly yield low bending loss.

6. Acknowledgements

This work was supported by grant 107T569 from TUBITAK, the Scientific and Technological Research Council of Turkey. The computations were performed on the ULAKBIM cluster at TUBITAK and on UYBHM cluster at Istanbul Technical University. For the time-

domain simulations, we used the publicly available software MEEP[17] which employs the Finite Difference Time Domain method[18].

1. J. C. Knight, T. A. Birks, P. S. Russell, and D. M. Atkin, "All-silica single-mode optical fiber with photonic crystal cladding" Opt. Lett. **21**, 1547-1549 (1996).
2. S. Y. Lin, E. Chow, S. G. Johnson, and J. D. Joannopoulos, "Demonstration of highly efficient waveguiding in a photonic crystal slab at the 1.5-μm wavelength," Opt. Lett. **25**, 1297-1299 (2000).
3. M. Tokushima, H. Kosaka, A. Tomita, and H Yamada, "Lightwave propagation through a 120 degrees sharply bent single-line-defect photonic crystal waveguide," Appl. Phys. Lett. **76**, 952-954 (2000).
4. M. Bayer, A. Forchel, T. L. Reinecke, P. A. Knipp, and S. Rudin, "Confinement of light in microresonators for controlling light-matter interaction," Phys. St. Sol. A-App. Res. **191** ,3-32 (2002).
5. S. Boscolo, M. Midrio, and C. G. Someda, "Coupling and decoupling of electromagnetic waves in parallel 2-D photonic crystal waveguides," IEEE J. Quan. El. **38**, 47-53 (2002).
6. S. H. Fan, P. R. Villeneuve, J. D. Joannopoulos, and H. A. Haus, "Channel drop filters in photonic crystals," Opt. Exp. **3**, 4-11 (1998).
7. S.Hughes, L. Ramunno, J. F. Young, and J. E. Sipe, "Extrinsic optical scattering loss in photonic crystal waveguides: Role of fabrication disorder and photon group velocity," Phys. Rev. Lett. **94**, 033903 (2005).
8. E. Kuramochi, M. Notomi, S. Hughes,1, A. Shinya, T. Watanabe, and L. Ramunno, "Disorder-induced scattering loss of line-defect waveguides in photonic crystal slabs," Phys. Rev. B **72**, 161318 (2005).
9. H. Taniyama, M. Notomi, and Y. Yoshikuni, "Propagation characteristics of one-dimensional photonic crystal slab waveguides and radiation loss," Phys. Rev. B **71**, 153103 (2005).
10. H. S. Sözüer and K. Sevim, " Robustness of one-dimensional photonic band gaps under random variations of geometrical parameters," Phys. Rev. B **72**, 195101 (2005).
11. A. Chutinan and S. Noda, "Waveguides and waveguide bends in two-dimensional photonic crystal slabs ," Phys. Rev. B **62**, 4488-4492 (2000).
12. A. Chutinan, M. Okano, and S. Noda, " Wider bandwidth with high transmission through waveguide bends in two-dimensional photonic crystal slabs," Appl. Phys. Lett. **80**, 1698-1700 (2002).
13. I. Ntakis, P. Pottier, and R. M. De la Rue, " Optimization of transmission properties of two-dimensional photonic crystal channel waveguide bends through local lattice deformation," J. App. Phys. **96** 12-18, (2004).
14. M. Notomi, A. Shinya, K. Yamada, J. Takahashi, C. Takahashi, and I. Yokohama, "Structural tuning of guiding modes of line-defect waveguides of silicon-on-insulator photonic crystal slabs," IEEE J. Quant. Elec., **38**, 736-742 (2002).
15. T. P. White, L. O'Faolain,J. T. Li, L. C. Andreani, T. F. Krauss, "Silica-embedded silicon photonic crystal waveguides," Opt. Exp. **16**, 17076-17081 (2008).
16. H.S. Sözüer, J.W. Haus, and R. Inguva, "Photonic Bands - Convergence problems with the plane-wave method," Phys. Rev. B **45**, 13962-13972 (1992).
17. A. Farjadpour, D. Roundy, A. Rodriguez, M. Ibanescu, P. Bermel P, J. D. Joannopoulos, S. G. Johnson, and G. W. Burr, "Improving accuracy by subpixel smoothing in the finite-difference time domain," Opt. Lett. **31**, 2972-2974 (2006).
18. See, for example, A. Taflove and S. C. Hagness, *Computational Electrodynamics: The Finite-Difference Time-Domain Method*, 3rd ed. (Artech House Publishers, 2005).